JOURNAL OF MATERIALS SCIENCE 24 (1989) 4225–4228

# Defects induced by $P^+$-implanted in silicon

YAN YONG, LI QI, FENG DUAN
*Laboratory of Solid State Microstructures and Department of Physics, Nanjing University, Nanjing, China*

WANG PEI DA
*Institute of Semiconductor, Academia Sinica, People's Republic of China*

SUN HUI LING
*Center of Microelectronics, Academia Sinica, People's Republic of China*

Cross-section transmission electron microscopy (X-TEM) has been used to show the microstructures and the defects in $P^+$-implanted (1 0 0) silicon crystals. $P^+$ implantation was done at room temperature with the energy of 150 keV and the dose of $1 \times 10^{15}\,cm^{-2}$. High resolution electron microscopy (HREM) image of (0 1 $\bar{1}$) slice shows that there are an amorphous layer 110 nm below the incident surface of specimen with thickness of about 100 nm, and two imperfect layers located symmetrically on each side of the amorphous layer in which there are various kinds of defects. {1 1 1} stacking faults and stacking fault tetrahedra are found near the amorphous layer, and {3 1 1} defects are far away from the layer. The interfaces between the amorphous and the imperfect layers are rough, the substrate, however, remains perfect.

## 1. Introduction

Recently, decreasing the device geometries in very large-scale integration and ultra large-scale integration devices presents many challenges for the silicon technologist, more and more interests has been shown in experimental [1, 2] and theoretical [3, 4] studies of structures of ion-implantation because of the number of advantages in this field. One aspect of these studies involves amorphization and defects induced by the implantation. If the electrical quality of the material is considered, then the spatial distribution, the density and the behaviour of the defects induced by ion-implantation are important issues [1–4]. However, the microstructure, especially the characterization of the defects, is still not clear. In this paper, the damage induced by $P^+$ implantation in silicon is studied by HREM. The type, configuration and distribution of the defects at different depths, and the microstructures at the amorphous layer and on the interface between the amorphous layer and the crystalline zone are shown.

## 2. Experimental details

The $P^+$ implantation was done at 150 keV with a dose of $1 \times 10^{15}\,cm^{-2}$ at room temperature on a (1 0 0) silicon slice. HREM observations were performed with a JEM-4000EX electron microscope (400 kV). X-TEM samples were made from strip ends corresponding approximately to the centre of 3 mm diameter wafer. For HREM analysis, X-TEM samples were prepared with a beam direction along (0 1 $\bar{1}$) which is perpendicular to the surface of (1 0 0) silicon slice. The higher accelerating voltage of JEM-4000EX means that the HREM image can be observed in the thicker area of the sample, which is very helpful in the study of the distribution of the different kinds of the defects at different depths in ion-implanted samples.

## 3. Results

Fig. 1 is a X-TEM micrograph of the implanted material and shows four layers with different structures. From the ion-incident surface, the first layer (A) is monocrystalline silicon with thickness of about 100 nm in which there is a large amount of different kinds of defects, the second (B) is the amorphous layer about 110 nm, the third (C) is also crystalline silicon, containing many defects like the layer (A) and the fourth (D) is the perfect crystal substrate.

The interfaces between the amorphous and the imperfect crystalline layers (A–C) are extremely rough. High resolution X-TEM micrographs (Fig. 2) of the A–C interface show that the contrast observed

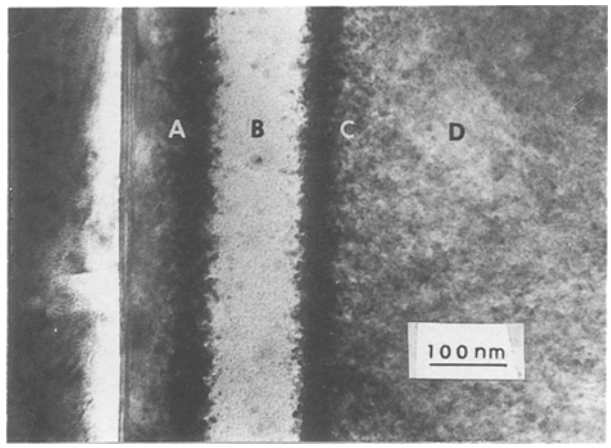


*Figure 1* A (0 1 $\bar{1}$) X-TEM micrograph of as-implanted (1 0 0) silicon sample at room temperature with 150 keV $P^+$ with dose of $1 \times 10^{15}\,cm^{-2}$.

0022–2461/89 $03.00 + .12 

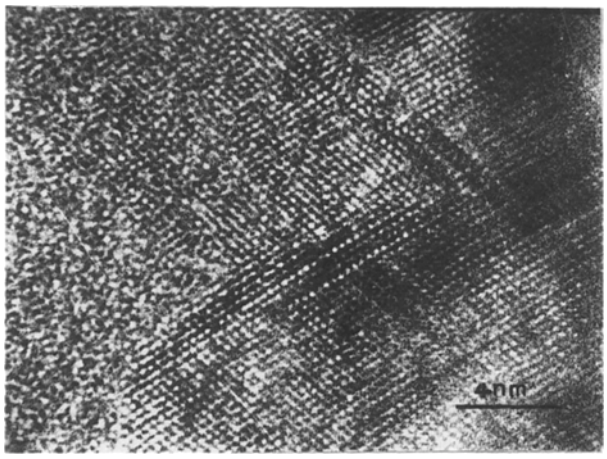


*Figure 2* A cross-sectional HREM image of the interface between imperfect crystalline layer (C) and the amorphous layer (B).

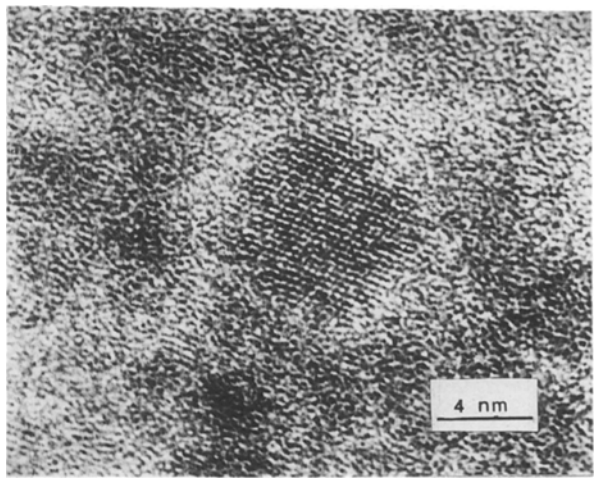


*Figure 3* HREM image of the crystallites in the amorphous layer (B).

during axial illumination in conventional X-TEM truly results from the contrast differences between crystalline and amorphous material. It was found that the A–C interface was almost wave-like with an amplitude of about 10 nm. The V-shaped open triangle consisting of (1 1 1) and ($\bar{1}$ 1 1) planes were often observed in the imperfect silicon layers near the A–C interfaces. The HREM image of the layer (B) shows that this layer is also amorphous material. Some crystallites are discernible (Fig. 3) when imaged at high resolution. They are randomly distributed in the layer and have the same crystallographic orientation as the silicon substrate. This shows that the amorphization induced by $P^+$ ion implantation in (1 0 0) silicon slice is incomplete in our experiment.

Fig. 4 is the HREM image of implanted silicon in the (0 1 $\bar{1}$) direction, which corresponds to the different layers in Fig. 1. This shows that there are various kinds of defects in the imperfect layers (A and C), which are located approximately symmetrically on each side of the amorphous layer. According to the kinds of the defects, the imperfect layers, A and C, may be divided into two layers, {1 1 1} stacking faults layer and {3 1 1} defects layer. Fig. 4a is the HREM image of the first layer (A). Near the $P^+$ incident surface, {3 1 1} defects can be seen, and near the A–C interface, a lot of {1 1 1} stacking faults and stacking fault tetrahedra are found. The distribution of the defects in the third layer (C) is similar to that of the first layer with inverted sequence of defects; the densities of {1 1 1} stacking faults and stacking fault tetrahedra are high near the A–C interface, {3 1 1} defects can be found far away from the amorphous layer. Their densities decrease with the increase of the distance from the A–C interface. The disordering of the lattice is often found in the imperfect layers. The crystalline substrate, however, remains perfect, as shown in Fig. 4b.

A typical image of a stacking fault tetrahedron observed along 0 1 1 is shown in Fig. 5a. The defect is revealed as a V-shaped open triangle consisting of (1 1 1) and ($\bar{1}$ 1 1) planes. When looking at the micrograph under grazing incidence in the (0 1 1) direction, that is, along the base of the open triangle, the rows of dots are seen to undergo a lateral shift away from the base of the triangle. The magnitude of the shift decreases with increasing distance from the base of the triangle and becomes zero near the top. The mismatch of lattice can be observed along the (1 1 1) direction. This image characteristic can be explained by assuming that the defect is a stacking fault tetrahedron consisting

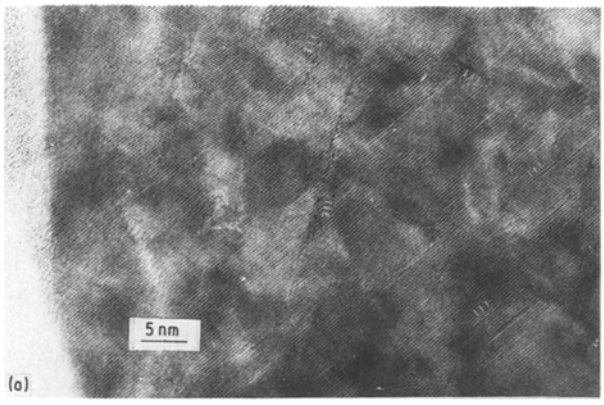


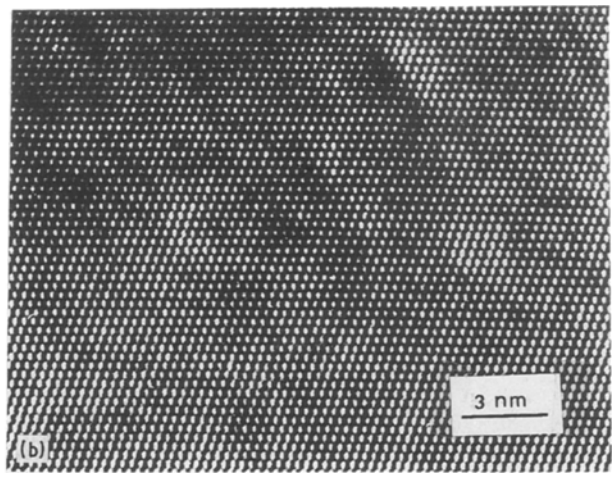


*Figure 4* (a) HREM image of the layer (A), near the incident surface, {3 1 1} defects; near the A–C interface, {1 1 1} stacking faults and stacking fault tetrahedra. (b) HREM image of the perfect silicon substrate.

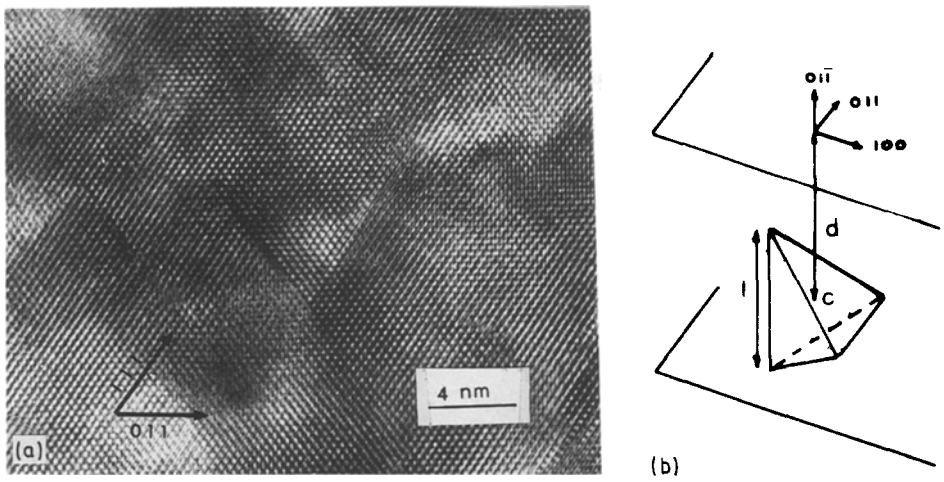


*Figure 5* (a) A typical image of a stacking fault tetrahedron along $\{0\,1\,\bar{1}\}$. It is revealed as a V-shaped open triangle. (b) The matrix of the stacking fault tetrahedron in the $(0\,1\,\bar{1})$ foil.

of stacking faults on the four $\{1\,1\,1\}$ planes, and with stair-rod dislocation having Burgers vector $\boldsymbol{b} = a/6\langle 0\,1\,1\rangle$, along the six $\langle 0\,1\,1\rangle$ edges. Fig. 5b is the matrix of the stacking fault tetrahedron in the $(0\,1\,\bar{1})$ foil. One edge is parallel to the direction of the incident electron beam. The two stacking fault planes on which the edge lies are also parallel to the incident beam. The V-shaped open triangles are formed by the two stacking fault planes. The observation and image simulation of the stacking fault tetrahedron in silicon had been given by Coene, Bender and Amelinckx [6]. The characteristics of our experimental image is similar to theirs. The nature of the defects, however, in Fig. 5a, either interstitial or vacancy, must be deduced by comparison with simulated images; this will be the subject of a future study.

The electron irradiation damage is quite large at 400 kV [7], thus the observation of HREM image must be done as quickly as possible. Figs 6a and 6b are the lattice images of defects in the same area near the surface of the sample before and after electron beam irradiation, respectively. After 20 min, the $\{3\,1\,1\}$ defects disappear and $\{1\,1\,1\}$ stacking faults and the disordering are generated. It was found that the density of the defects increases with the time of irradiation.

Other effects of electron beam irradiation is recrystallization of the amorphous layer (B). A reverse transition from amorphous to crystalline was observed. Fig. 7 is an electron micrograph of the A–C interface after 40 min by electron beam radiation. It was noted that the width of the amorphous layer is only about 45 nm in the area irradiated. Solid-phase epitaxial regrowth of the amorphized layer can be observed by comparing with the area which had not been irradiated. The regrowth area is also imperfect and the new A–C interface is extremely irregular.

## 4. Discussions

The interpretation of ion-implantation experiments requires a knowledge not only of the incident ion locations within the target, but also of the partitioning of the incident energy into atomic (damage) processes and electronic (ionization) processes, as well as the distribution of this deposited energy within the target [3, 4]. The depth distribution of implantation ions is relatively symmetric. The energy-deposition distributions, however, are not generally asymmetric. However, they have an approximately symmetric distribution near the peak of damage [4] which is in qualitative agreement with our experimental results. In our

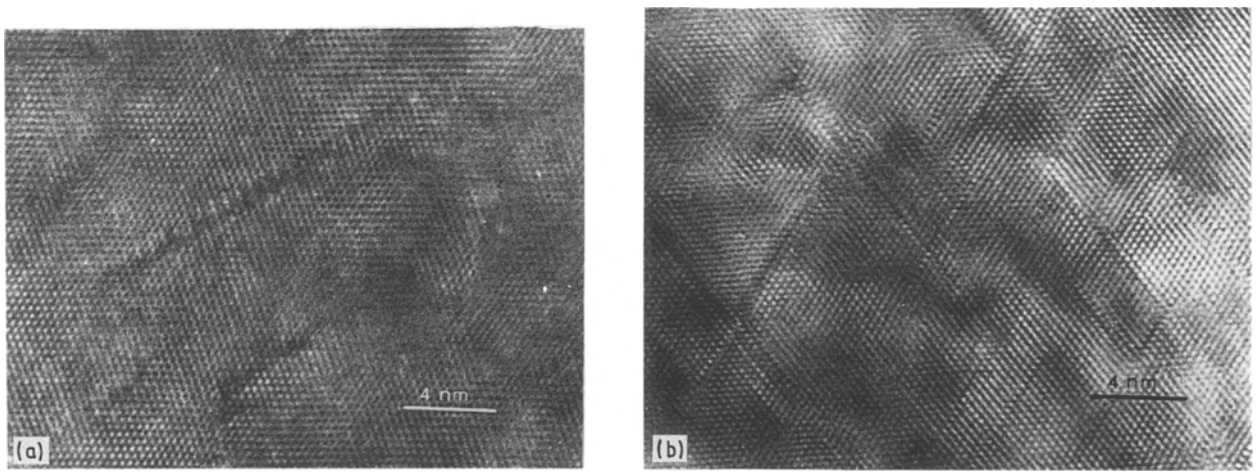


*Figure 6* (a) HREM image of the $\{3\,1\,1\}$ defects in imperfect crystalline layer (A) before electron beam irradiation. (b) After 20 min, the $\{3\,1\,1\}$ defects disappear and the $\{1\,1\,1\}$ stacking faults and the disordering are generated in the same area with Fig. 6a.

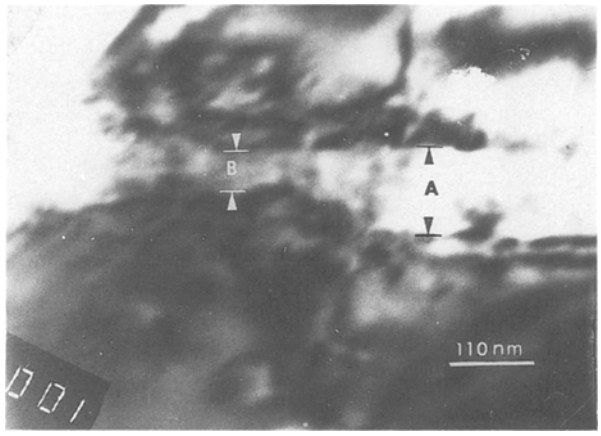


*Figure 7* The micrograph of the A–C interface after 40 min by electron beam irradiation. The width of the amorphous layer is reduced from 110 nm (A) to 45 nm (B) in the same area irradiated.

experiment, the damage sequence is found to be {3 1 1} defects, {1 1 1} stacking faults and stacking fault tetrahedra, the amorphous layer, {1 1 1} stacking faults and stacking fault tetrahedra, {3 1 1} defects and perfect substrate. In accordance with the normalized damage energy distribution, it can be expected that the energy to produce {1 1 1} stacking faults and stacking fault tetrahedra will be higher than that producing {3 1 1} defects. From the positions and characteristics of the defects distribution at different depth, using the above-mentioned hypothesis, the damages induced by electron beam irradiation may be interpreted. The energy deposited in silicon is increased with increasing the irradiation time, thus the {3 1 1} defects near the incident surface induced by $P^+$ implantation can be transformed to {1 1 1} stacking faults due to the electron beam irradiation. At the same time, the densities of the {1 1 1} stacking faults and the stacking fault tetrahedra are also increased and further disordering of the lattice is produced in the area near the A–C interface. The electron beam irradiation also results in the rise of temperature of the specimen. This effect is similar to a thermal annealing for the amorphous layer (B) which results in the solid-phase epitaxial regrowth.

## Acknowledgement

We are grateful to Dr. Chen Jun for useful discussions.

## References

1. D. M. MAHER, R. V. KNOELL, M. B. ELLINGTON and D. C. JACOBSON, *Mat. Res. Soc. Symp. Proc.* **52** (1986) 93.
2. W. T. DONLON, J. V. JAMES, J. C. BOMBACK, C. R. HUO and C. C. WANG, *Ultramicroscopy* **22** (1987) 305.
3. K. B. WINTERBON, *Radiot. Eff.* **13** (1972) 215.
4. DAVID K. BRICE, *J. Appl. Phys.* **46** (1975) 3385.
5. Y. TSUBOKAWA, M. KUWABARA, H. ENDOH and H. HASIMOTO, in Proceedings of the XIth International Congress on Electron Microscopy, Kyoto, August, 1986, edited by T. Imuka, S. Maruse and T. Suzuki (The Japanese Society of Electron Microscopy, Tokyo, 1986) p. 955.
6. W. COENE, H. BENDER and S. AMELINCKX, *Phil. Mag. A* **52** (1985) 369.
7. M. KUWABARA, H. ENDOH, Y. TSUBOKAWA, H. HASHIMOTO, Y. YOKOTA and R. SHIMIZU, in Proceedings of International Symposium on "Behavior of Lattice Imperfections in Materials – *In Situ* Experiments with HVEM", Osaka, November (1985) 341.

*Received 2 September 1988*
*and accepted 24 February 1989*